Impact of 802.15.4 Radio Antenna Orientation on UAS Aerial Data Collection

Michael Nekrasov, Maxton Ginier, Ryan Allen, Irina Artamonova*, Elizabeth Belding

UC Santa Barbara, {mnekrasov, maxton, rallen00, ebelding}@cs.ucsb.edu

*UC San Diego, School of Medicine, iartamonova@ucsd.edu

Abstract—This work uses experimental measurements to study the impact of network configuration and flight planning on Unmanned Aircraft System (UAS) assisted data collection in a 2.4GHz IEEE 802.15.4 outdoor aerial testbed. Our paper builds on previous work in UAS data collection from 802.15.4 outdoor sensor networks by conducting a novel investigation of the impact of antenna orientation on transceivers with external straight wire antennae. We study the effects of toroidal radiation and antenna polarization on signal strength, and we compare external antenna configurations to the commonly used embedded coiled antenna modules. We model our data using a Zero Inflated Negative Binomial (ZINB) model. For each hardware configuration and orientation, we identify the optimal altitude to fly a UAS. Our results show that choosing antenna configuration (including type and orientation) for an IoT network depends on the intended UAS collection flight plan.

Index Terms—Internet of Things; 802.15.4; UAS; UAV; drone; sensor network; wireless networks; aerial networks; experimental measurements

I. INTRODUCTION

Internet of Things (IoT) devices and sensors proliferate across a wide domain of applications, ranging from home automation to environmental monitoring. The IEEE 802.15.4 standard is one of the most common communication protocols for IoT devices, in part because standards designed for complex computing devices do not fit the power and network topology for many IoT applications. For example, the IEEE 802.11 (WiFi) standard consumes considerable power and is ill-suited for the periodic, low bandwidth communication typical of IoT networks. In contrast, 802.15.4 is optimized for low power, low data rate node-to-node connectivity inside a local sensor network [1]. However, remote sensor networks still require an Internet gateway for broader Internet access. In areas without Internet access, due to lack of infrastructure or due to infrastructure damaged in events such as natural disasters, alternate Internet access technologies are necessary.

One emerging approach to providing delay tolerant access to disconnected sensor networks utilizes Unmanned Aerial Systems (UASs). UASs already function in a number of rural applications, including automated ground surveying [2] and precision agriculture [3]. Most previous IEEE 802.15.4 research has focused on a flat, two dimensional network topography. However, interactivity between 802.15.4 and UASs occurs in a three dimensional space. This configuration poses unique challenges, such as a toroidal radiation and signal polarization, and generates new parameters for optimization, such as flight altitude and antenna orientation.

Past literature, presented in Section II, suggests antenna orientation between transmitter and receiver significantly impacts network quality. 802.15.4 hardware comes in various types, such as coiled compact embedded antennae printed directly on the circuit board and external straight-wire antennae. In our previous analysis of UAS data collection from 802.15.4 ground-based devices, we discovered that embedded coiled antenna orientation of the transmitters and the receivers had little impact on signal strength [4]. However, we theorized that external antenna modules may be more sensitive to orientation and therefore might display previously observed behavior, such as toroidal radiation.

To our knowledge, this is the first paper to analyze the performance impact of antenna orientation in an outdoor rural aerial 802.15.4 network using external straight wire antennae. We study the effects of toroidal radiation and antenna polarization on signal strength. We compare external antenna configurations to the commonly used embedded coiled antenna modules. We model our data using a Zero Inflated Negative Binomial (ZINB) model. For each hardware configuration and orientation, we identify the optimal altitude to fly an UAS in our testbed. Our results show that the best choice of antenna configuration (including type and orientation) for an IoT network depends on the intended UAS collection flight plan. For example, in our study, we find that UAS flights with a horizontal displacement to transmitters less than 150 meters optimize when using vertically oriented transmitters with internal antennae and a UAS flight altitude of 150-250 feet. On the other hand, UAS flights with a horizontal displacement to transmitters exceeding 150 meters optimize when using vertical transmitters with external antennae and are not sensitive to flight altitude.

II. RELATED WORK

The performance of the 802.11 network standard has received extensive study. Work in 802.11 suggests that communication with highly mobile UASs, operating in three dimensional space, involves unique challenges. For example [5] and [6] revealed that the high mobility of UASs results in poor 802.11 performance due to chipset limitations, and the large volume of data that is usually transmitted over 802.11. [7] and [8] demonstrated that 2.4GHz 802.11 consumer hardware is affected by antenna orientation in the aerial context due to the toroidal radiation patterns of the omni-directional dipole antennae. From the similarity of the physical layer

between 802.15.4 and 802.11 radios, we reasonably expect 802.15.4 to evince the same affects of toroidal radiation of the omni-directional dipole antennae of IoT devices in a three-dimensional environment.

Work in 802.15.4 has largely focused on two-dimensional topography, common to terrestrial networks. For example, [9] examined 802.15.4 signal propagation, while [10] examined person-to-person communication over 802.15.4, and found mobility to be challenging in an 802.15.4 network. Additionally, [11] examined enhancements to two dimensional movement and stationary 802.15.4 roadside sensors, and [12] evaluated 802.15.4 indoor and outdoor performance in terms of error rate and RSSI.

In contrast, research on 802.15.4 in three dimensional space is more sparse. While [13] found that 802.15.4 devices are sensitive to antenna orientation, their measurements were collected on sensors within 3m of each other and therefore do not scale well to UAS data collection scenarios that measure distances in the hundred of meters [14]. On the other hand, [15] looks at the performance of Flying Ubiquitous Sensor Networks (FUSN), and aerial data collection in hard to reach, remote locations. In addition, [16] provides a simulation of a sensor network with hundreds of nodes, but real-world topography and obstruction was not considered in their methods.

Our own work [4], [17] shows that simulated assumptions are not matched by empirical measurements of real aerial 802.15.14 networks. This work investigated aerial data collection of an outdoor 802.15.4 network using radios with embedded PCB antennae, common to IoT devices and examined how topography, altitude, distance, and obstruction affect network quality. While the coiled antenna demonstrated insignificant differences in performance from radio module orientation, we did not explore whether the orientation of an external antenna would have a more pronounced impact on network quality.

Our paper builds on previous work in UAS data collection from 802.15.4 outdoor sensor networks by conducting a novel investigation of the impact of antenna orientation on transceivers with external straight wire antennae. This paper uses experimental measurements to study the impact of network configuration and flight planning on UAS assisted data collection in an outdoor aerial testbed.

III. METHODS

The results of this paper are based on experimental data collected using an outdoor aerial testbed at Coal Oil Point Reserve near the University of California, Santa Barbara in March, September, and October 2019. We deployed 802.15.4 transmitters broadcasting packets at 500 ms intervals to a mobile UAS. We varied radio hardware, antenna orientation, altitude, distance, and amount of obstruction. We performed multiple repeated measures, varying sensor placement and UAS flight path.

A. Equipment

The experiments used a single UAS and two sets of 802.15.4 Digi 2.4GHz Xbee3 radios, a set of transceivers with

(a) Horizontal Internal   (b) Vertical Internal   (c) Obstructed External

(d) Horizontal External   (e) Vertical External   (f) Elevated External   (g) Elevated Internal
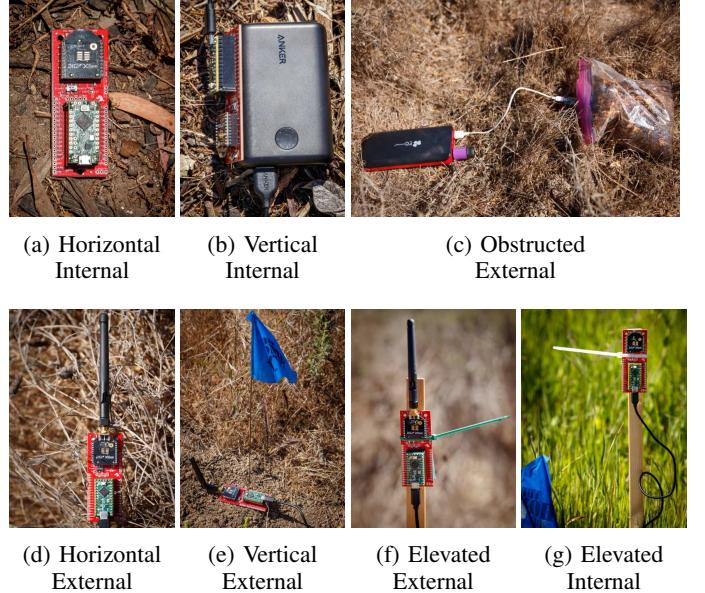
Figure 1: Transmitter configurations.

integrated antennae, and a set of transceivers with external antennae. The transceivers used the Digi XB3-24-2003-TH implementation of the IEEE 802.15.4 protocol, on a frequency of 2.420GHz transmitting at 8dBm. The specifications for both sets of transceivers advertise an outdoor range of 1200 m at a power of 8dBm and a receiver sensitivity of -103dBm [18]. To evaluate the choice of antenna type, we first conducted experiments utilizing radio modules with integrated antennae, then swapped for external antenna modules as described in this section.

Integrated Antenna Modules: The first set of six transceivers comprised Digi WRL-15126 XBee3 using PCB antennae; we refer to these as *integrated antenna* modules. These radios are popular due to their compact form factor. Because the antennae are integrated into the circuit board, changing antenna orientation also rotates the entire radio module. For transceivers with integrated antennae, in the *horizontal orientation* the radio module circuit board is parallel to the ground, as shown in Figure 1a. In the *vertical orientation* the circuit board is perpendicular to the ground, as shown in Figure 1b.

External Antenna Modules: The second set of six transceivers were Digi WRL-15130 XBee3 with an external WRL-00145 RP-SMA 2.2 dBi Duck Antenna [19]; we refer to these as *external antenna* modules. The external antennae allow control of antenna orientation independent of the radio module. For transceivers with external antennae, in the *horizontal orientation* the antenna is parallel to the ground, as shown in Figure 1d. In the *vertical orientation* the antenna is perpendicular to the ground, as shown in Figure 1e.

Transmitters: For each set of Xbee3 radio modules, four of the six were designated as transmitters. These were mounted on SparkFun XBee Explorer boards controlled by a SparkFun Teensy LC, powered by external USB battery packs from vary-

Figure 2: DJI Matrice 100 used in our experiments.

ing vendors via a USB-to-Serial converter on the Teensy LCs. For both antenna variants, the transmitters were programmed to broadcast 23 byte packets every 500 ms. The payload of the packets consisted of a randomly generated floating point number (simulating numerical data of a potential attached sensor), as well as device and packet identifiers.

At the start of each experiment, the transmitters were randomly placed approximately 10 to 15 meters apart, avoiding obstruction within the 15cm vicinity of each transmitter. The latitude and longitude of the transmitter were recorded manually via a GPS.

Each of the four transmitters was, as shown in Figure 1, deployed in one of four unique configurations: horizontal, vertical, elevated, and obstructed. The *horizontal transmitter* was placed on the ground with its antenna in the horizontal orientation (as previously defined). Similarly, the *vertical transmitter* was placed on the ground with its antenna in the vertical orientation. The *elevated transmitter* was mounted to a pole one half meter above the ground with its antenna in the vertical orientation. The *obstructed transmitter* was laid flat on the ground with its antenna, in a horizontal orientation, covered with one quart of debris consisting of dirt and wood chips.

Unmanned Aircraft System: Packets broadcast by the transmitters were collected using an unmanned aircraft system. For the UAS, we utilized a DJI Matrice 100 quad-copter, as shown in Figure 2. The Matrice 100 communicates with a remote control at 5.725 - 5.825 GHz, which is outside the frequency range of the 2.4GHz XBee nodes. The UAS was flown manually with no attached camera. A Raspberry Pi 2 - Model B served as an on-board computer. The location of the UAS was recorded from the Matrice 100 on-board GPS, sampling at a rate of 50Hz and using a UART connection to the Pi.

When evaluating antenna type we used a matching pair of recievers on the UAS. So when evaluating internal antennae, four of the six XBee3 radios with internal antennae were used as ground based transmitters and two of the six were mounted to the bottom of the UAS. Likewise for the external antennae tests. These modules acted exclusively as receivers set to capture only. We oriented the antennae of the receiver in two configurations. The *horizontal receiver* had its antenna in a horizontal orientation, while the *vertical receiver* had its

antenna in a vertical orientation. The two XBees forwarded packets to the Pi via a USB connection.

We flew the UAS over the transmitters at an average speed of four meters per second. The exact flight path and speed varied due to manual execution under varying wind conditions. Because the United States Federal Aviation Administration (FAA), which governs the airspace over our testbed, regulates altitude in feet, we represent altitude (relative to ground level at the start of flight) in feet, while keeping displacement in meters. Flights for the integrated antennae were at altitudes of 50 ft, 100 ft, 200 ft, 300 ft, and 400 ft at horizontal displacement of up to 250-325 meters from the closest transmitter to the UAS. When conducting flights for the external antenna modules, we saw an improved reception range for certain configurations and altered our flight plan to include altitudes of 150 ft and 350 ft and horizontal displacement of up to 650 meters. As the FAA limits max altitude to 400 feet, we restricted our maximum experimental flight altitude to match (the EU similarly limits flight to 120 m ≈ 394ft).

B. Experimental Area

The experiments took place outdoors at Coal Oil Point UC Reserve, a coastal grassland near the university. The experiments were conducted in a relatively flat area with some ground level obstruction due to tall grass and shrubs. The transmitters were placed so that the 15cm around each transmitter was clear of any obstruction, in areas with no tall shrubs in the 2m vicinity. For UAS horizontal displacement of over 350 meters, tall clusters of trees lined the sides of the flight path, however the UAS kept a line of sight corridor to the deployment area.

C. Measurements

Received Signal Strength Indication: Received Signal Strength Indication (RSSI) is a common indicator of signal strength; in fact it is often the only signal quality metric reported by radio hardware. As a result, prior research of air to ground networks has relied on RSSI as a key indicator of network performance [6]–[8].

However, as our past work has shown [4], [17], RSSI may not be the ideal indicator for 802.15.4. RSSI is typically calculated by the receiver from successfully received packets. When conditions are poor and RSSI is low, the packets may not be received by the receiver and, as a result, their RSSI may not be recorded. Therefore, in past outdoor aerial 802.15.4 measurements, we observed that the mean of the received RSSI remains relatively consistent despite changes to experimental variables, such as adding obstruction. In contrast, with fixed transmission frequency, significant shifts to the total number of received packets suggest significant differences in network performance between configuration scenarios not accounted for by RSSI.

In this work, while we provide an overview of RSSI for comparability to past work, we focus on packet reception as a more definitive network quality metric for the outdoor aerial 802.15.4 data collection use case.

Packet Reception Rate: Unlike other applications, where throughput, latency, and jitter are the principle metrics of performance, IoT applications are often delay tolerant and do not saturate network bandwidth. Instead, IoT networks try to minimize power consumption, especially outdoors where there may not be access to grid power. Similarly a UAS has a limited battery, and hence limited flight time. Therefore to maximize performance of an aerial data connection, we seek to minimize the number of failed transmissions. Accordingly, we measure the packet reception rate (PRR), which is the number of packets received divided by the calculated number sent, as the principle metric of 802.15.4 IoT network performance:

$$\text{PRR} = \frac{\text{number of packets received}}{\text{time of UAS in sector} * \text{transmission rate}}$$

Because PRR only makes sense over an aggregate of readings, we group the experimental data by horizontal displacement from the corresponding transmitter into concentric circular sectors, 25m wide, radiating out from each transmitter, keeping other experimental variables separate. To determine the sector into which a packet from a particular transmitter falls, we compare the UAS's on-board GPS with the manually recorded transmitter location. We estimate the number of packets sent by a transmitter by taking the product of the transmission rate and the time-in-sector occupied by the UAS. We drop measurement windows where fewer than five packets were sent.

D. Modeling Packet Reception Rate

To study the effect of each variable on PRR, we model the expected mean PRR using Zero Inflated Negative Binomial (ZINB). From past work [17], we found that ZINB was the best fitting model, as it accounts for the over-dispersion and high number of PRRs at zero from locations and altitudes that never receive a packet. We therefore model both the chances that a packet is received at all and the estimated number of packets received. As the internal and external data sets had some experimental differences (the internal antenna had fewer displacement bins, and one fewer altitude), we constructed two independent ZINB models for each antenna type. We assessed the goodness of fit for our ZINB models by Scaled Pearson Chi-Square criteria, which were close to one and by the Full Log Likelihood criteria. We also compared the observed relative frequencies of the various counts to the maximum likelihood estimates of their respective probabilities. We found that our models were a good fit for the observed data.

To prepare for modeling we aggregated our readings into sectors, as discussed in the last section. We separated our data into internal and external antennae. We then randomly divided each group data into two sets: 60% was designated as a *training set*, while the remaining 40% was designated as a *test set*. We used a ZINB model with the number of received
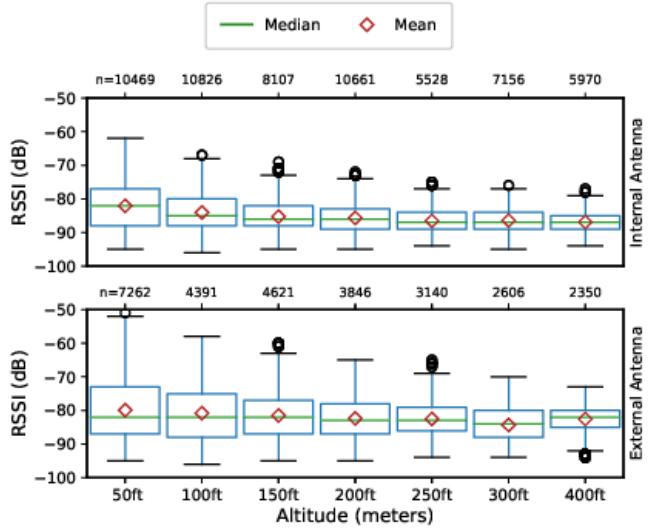

Figure 3: RSSI by altitude grouped by antenna type. The number of received packets are presented above as *n*.

packets as the outcome. For the model of external antennae we set displacement as a categorical variable with 25 groups (25m to 625m), altitude as a categorical variable with 8 groups (50 ft to 400 ft). For the model of internal antennae we grouped displacement as 11 groups (25m to 275m) and altitude with 7 groups (omitting 350 ft). For both models the transmitter-receiver configuration was 8 groups *(Vertical & Horizontal Receivers paired with Horizontal, Elevated, Obstructed & Vertical Transmitters)* as fixed covariates for both parts of our model. We used a natural logarithm of sent packets as an offset in the NB part of the model and control for the number of sent packets in the ZI part of the model.

IV. EVALUATION

A. RSSI

For each received packet we logged the RSSI reported by the receiver modules on the UAS. In particular, we examined how RSSI changed based on antenna type (internal vs. external), antenna orientation of the transmitter and receiver, amount of obstruction, and altitude.

Altitude: To examine the impact of altitude, we group the data by antenna type and altitude. We present the distribution by group as a box plot in Figure 3. These distributions include data from all horizontal displacements and transmitter configurations. The top plot shows the distribution of observed measurements from the set of transmitters with internal antennae, and the bottom shows those with external antennae.

The median and mean RSSI for both internal and external antenna remained close to one another with fluctuations within $\pm 2dB$ for each altitude. The minimum RSSI values remained likewise fixed. However the interquartile ranges shrank at higher altitudes, as the UAS increased in total vertical distance from the transmitters. Notably the external antennae'
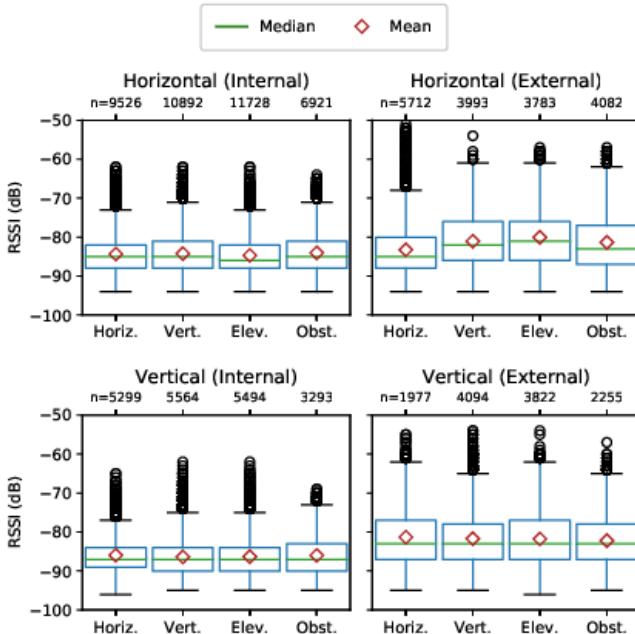
Figure 4: RSSI distribution grouped by antenna type and transmitter configuration. The number of received packets are presented above as *n*.

maximum RSSI is $\approx 10dB$ better than the internal antennae, across all altitudes.

Transmitter Configuration: To examine the impact of antenna orientation and obstruction, we group the data by antenna type, orientation, and obstruction. We present the resulting box plot in Figure 4. The two left plots show results from internal antenna modules for both the transmitter and receiver, while the two plots on the right show those for external modules. The top two plots correspond to horizontal antenna orientations for the receivers, while the bottom two plots show vertical receiver orientation. Each of the four subplots show the four possible transmitter configurations: horizontal antenna orientation, vertical orientation, elevated transmitter with a horizontal orientation, and obstructed transmitter with horizontal orientation.

We can see that the mean and median RSSI across all conditions remain within $\pm 3dB$ of each other, with similar interquartile ranges. Overall, the external antennae perform better than the internal antennae; the majority of the packets are received with higher RSSI.

The internal antennae display unusual behavior in the performance of the elevated and obstructed transmitters, showing that, contrary to expectation, the obstructed transmitter performs better than the elevated transmitter. When controlling for the number of packets sent, we found that while the obstructed transmitter RSSI is not significantly different, the obstructed transmitter successfully delivered less than half the number of packets. This strongly suggests that RSSI is not a reliable indicator of network performance for this application.

B. PRR

Because RSSI does not provide a comprehensive look at network performance, we focus the majority of our analysis on packet loss by examining PRR. As explained in Section III-C, we group our observations into 25m sectors. In our analysis we omit observations where fewer than five packets were sent, resulting in 12,891 total observations (8,591 observations for the external antenna set and 4,300 observations in the internal antenna set). Roughly 36% of the groups received at least one packet.

A heatmap of the observed PRR grouped by antenna type, antenna orientation, altitude, and horizontal displacement, averaged across multiple runs, is shown in Figure 5. Results for the internal antenna modules are shown in the left (Figures 5a and 5c), while those of the external modules are shown in the right (Figures 5b and 5d). Each figure is broken down by transmitter configuration with the color of each square representing the average PRR of a horizontal displacement sector at a particular altitude. White squares indicate fewer than five packets were sent at those variable conditions and so are omitted from the heatmap.

The internal antenna flights have fewer (displacement, altitude) pairs filled than the external antennae. As we performed those experiments first, we tailored the flight plan to preliminary results on that hardware type. As we found near total loss at distances greater than 250 meters, we limited our flights around that range. In contrast, the external antennae showed greater reception range, so we tripled our maximum horizontal displacement (further displacements was limited by restrictions on our airspace) and added an additional altitude measure of 350 ft. Due to the significantly increased flight times from the increased horizontal range, we restricted altitude to 50, 100, 150, 200, 250, 300, 350, and 400 feet.

Modeling PRR: From the training set, we constructed a pair of ZINB models of PRR (one for internal and one for external antennae), as described in Section III-D. Using these models, we can predict (based on input variables of hardware type, antenna orientations of transmitter and receiver, horizontal displacement, and altitude) the expected mean PRR. We utilize these models to study the effects of each variable on PRR. Network planners could likewise use this type of model, perhaps expanding the training set to fit more geographic topographies, to plan out sensor network equipment deployment and aerial data collection.

We can turn the ZINB model, which predicts a rate, into a binary classifier, predicting when at least one packet will be received, by specifying a threshold below which we expect the packet to be lost. We verify the resulting classifier based on the test set. We present a Receiver Operating Characteristic (ROC) curve of the ZINB for both models executed on the *test set* in Figure 6. This displays the possible true and false positive rates based on threshold choices. For example, given an external antenna and a PRR threshold of 30%, the resulting binary classifier correctly identifies 77% of the observations with a recall of 78% and specificity of 76%.
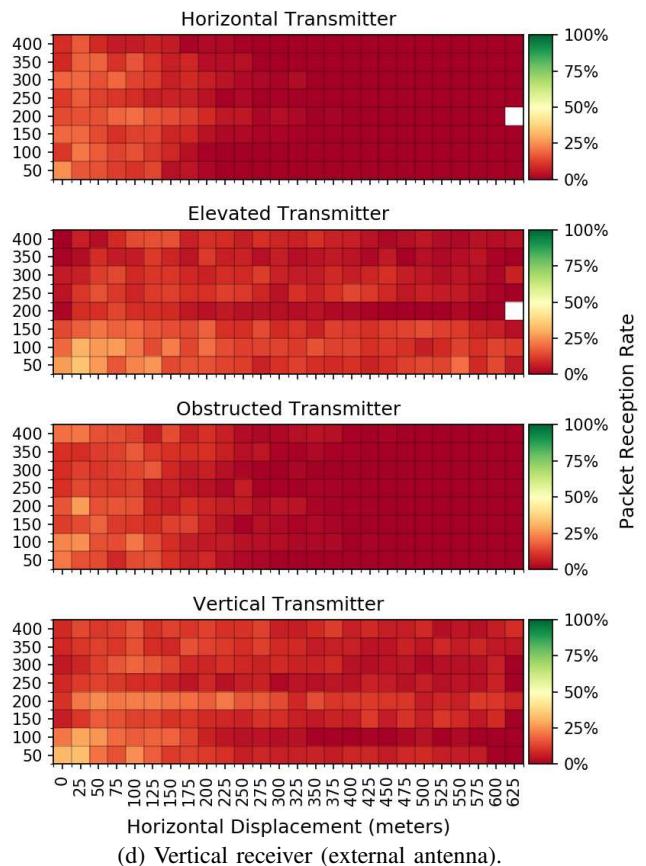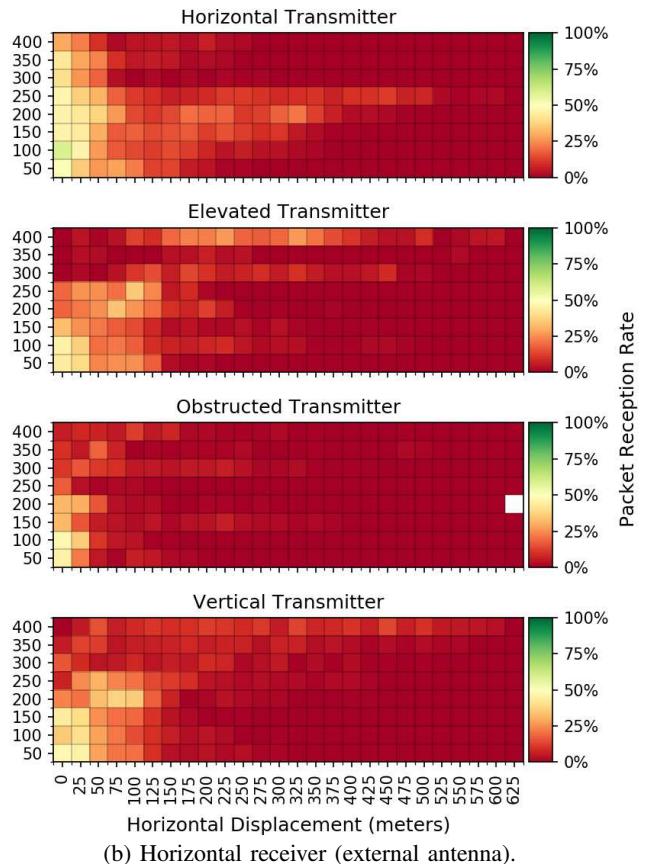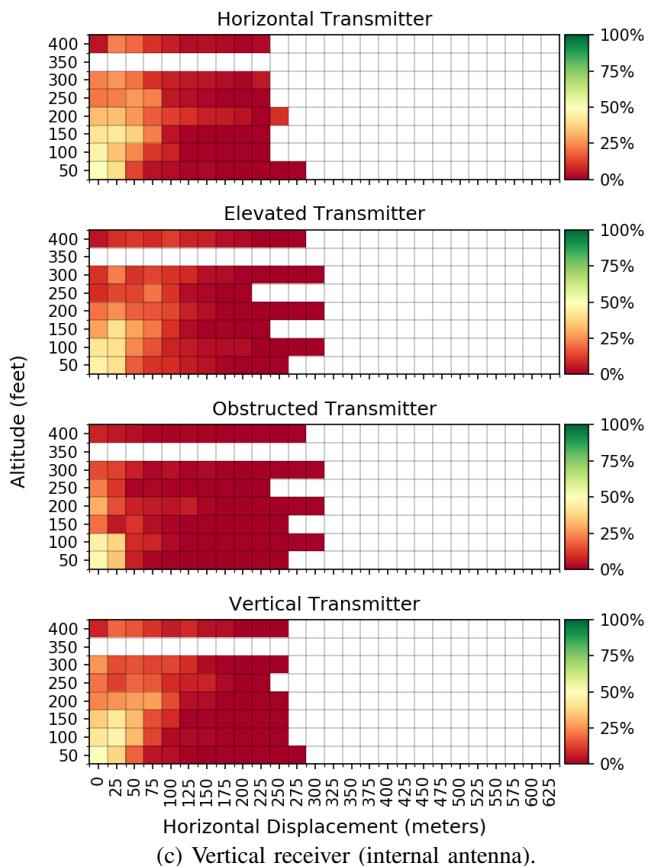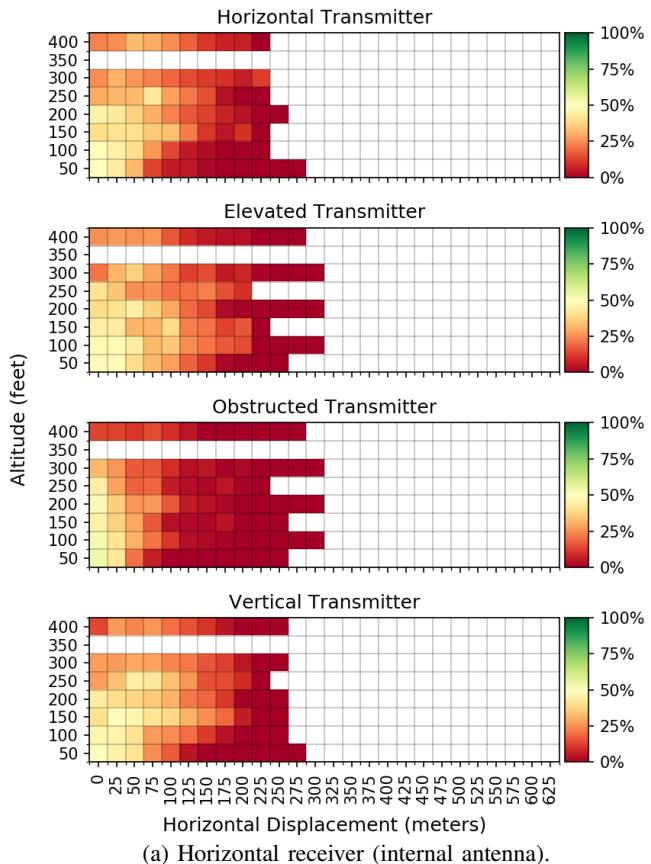
Figure 5: Observed packet reception rates grouped by altitude and 25m displacements from transmitter. Cells with fewer than five sent packets are left blank.

(a) Internal antenna model.   (b) External antenna model.
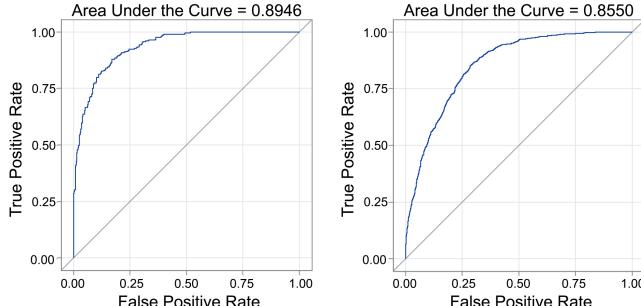
Figure 6: ROC curve for ZINB models evaluated on test sets.

A key focus of this study was to examine the difference between the internal coiled circuit board embedded antennae that we previously evaluated [4], [17] and the external straight wire antennae. To make this comparison, we examine the differences between the PRR of the four receivers (external horizontal, external vertical, internal horizontal, and internal vertical) across UAS altitudes and horizontal displacements. Due to limits in manpower, this work does not examine mixing transmitter and receiver antenna types (for example internal transmitter with external receiver). For this study, we assume that antenna types are homogeneous between transmitter and receiver; we will examine heterogeneous antennae types in future work.

Transmitter Configuration: First, we compared the PRR based on transmitter configuration, examining antenna type, obstruction, altitude, and orientation. In Figure 7, we present plots from the model for the PRR grouped by altitude and displacement, separated by internal and external antennae.

The difference between configurations of transmitters with internal antennae was less stark than the external antenna models. For the internal antennae, as expected, the vertical elevated antenna with the horizontal receiver showed the highest PRR rate, followed by the vertical ground level antenna with the horizontal receiver, then followed by the vertical elevated with a vertical receiver. The worst PRR was, again as expected, the horizontal obstructed transmitter with the vertical and horizontal receivers. This order held across altitudes and displacements.

For transmitters with external antenna modules, there was a higher variance in PRR by configuration. The vertical transmitters (both elevated and not) paired with the vertical receiver had a PRR nearly double that of the other antennae configurations. Unlike the internal antennae, for the external set, altitude did not make a difference on PRR. For the external set, the vertical transmitters outperformed the horizontal transmitters, particularly when paired with vertical receivers.

Interestingly, the obstructed horizontal transmitter had a higher PRR than the horizontal unobstructed transmitter when collected by the vertical receiver. The obstructed horizontal transmitter had the worst PRR when collected by the horizontal receiver.

Receiver Configuration: Next, we compare the PRR by receiver across all transmitter configurations of the matching antenna type. We present plots from the model for the PRR grouped by altitude and displacement in Figure 8. Overall, the receivers with internal antennae exhibited higher PRRs, regardless of orientation.

When examining the effect of receiver orientation, we found that for the internal antenna hardware, the horizontal receiver produced a better PRR across all altitudes and displacements than the vertical receiver. The behavior of the internal antenna modules is attributable to the mounting of the receivers. While the horizontal receiver was mounted on the bottom of the UAS, with clear line of sight to the ground at all times, the vertical receiver was mounted on the side of the UAS undercarriage with the mounting potentially interfering with line of sight at some angles.

The effect of receiver orientation on the external antenna modules is more complex. At smaller displacements ($< 100m$), the receiver with horizontal antenna orientation exhibited a higher PRR, while at greater displacements the vertical antenna had higher PRR.

Horizontal Displacement: As expected, PRR drops off as horizontal displacement between the UAS and transmitter increases, influenced by the inverse square law of signal strength decay. The internal antennae sets have an overall higher PRR at close displacements, but as displacement increases to 250 m, PRR falls to near zero. In contrast the external antennae, while overall yielding a lower PRR, still perform well at extreme distances of $> 600m$.

Altitude: For internal antenna modules, as seen in Figure 7a (right), collecting at altitudes of around 150 ft maximizes PRR (the exact optimal altitude depends on antenna configuration). In contrast, for the external antennae shown in Figure 7b (right), there is no optimal altitude. For external antennae higher altitude corresponds to a higher PRR up to the US FAA limit of 400 ft (likely there is an optimal altitude past this limit).

The toroidal radiation pattern of the external dipole antenna introduces additional considerations when selecting an altitude for UAS data collection. Dipole antennae radiate outwards, perpendicular to their orientation, with a cone of low signal strength at the tip of the antenna (the exact radiation pattern can be found in [19]). While overall lower horizontal displacements produce a higher PRR, for *vertical transmitters* there is a dip in PRR at displacements $< 100m$ for altitudes $> 200ft$. This is most clearly seen in Figures 5b and 5d. In contrast, external horizontal transmitters perform better across all altitudes at smaller displacements.

V. CONCLUSION

When evaluating the efficacy of an outdoor aerial assisted data collection strategy for a sensor network, network administrators need real-world models of optimum flight altitude, expected reception rates, and maximum effective horizontal

(a) Internal antennae.

(b) External antennae.
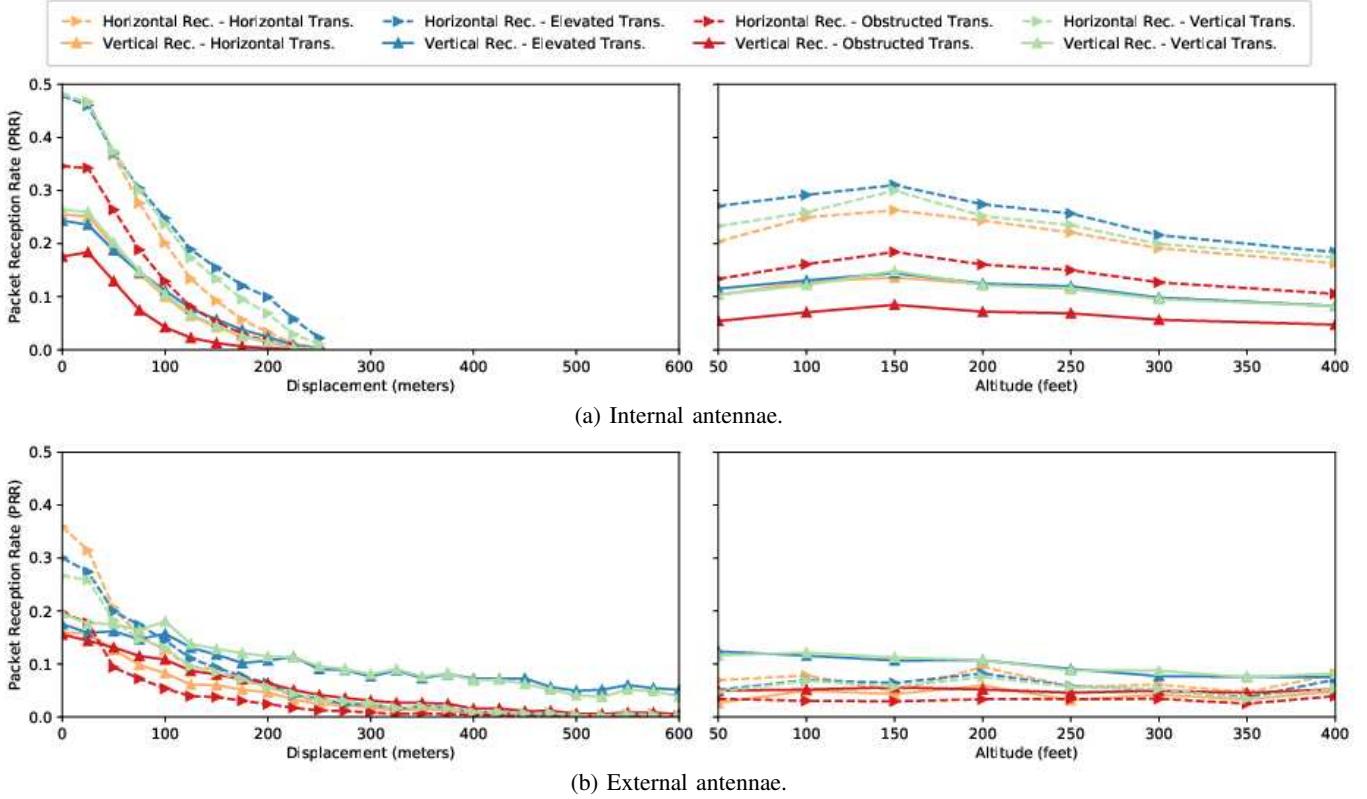
Figure 7: PRR grouped by altitude and displacement, varying antenna type and configuration.
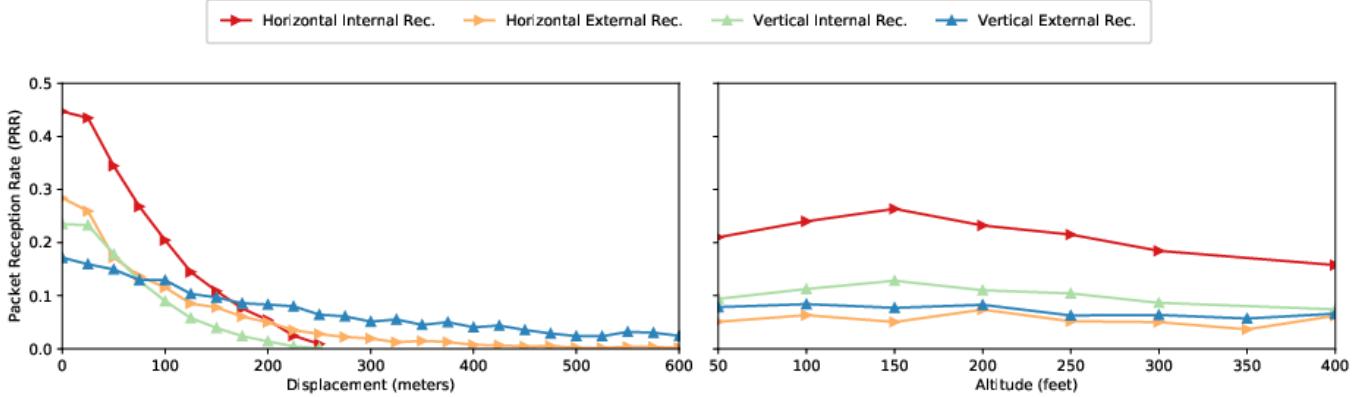

Figure 8: PRR grouped by receiver type.

displacement for reliable data reception. Our work provides a foundation for understanding 802.15.4 2.4GHz outdoor performance for three dimensional network communication using physical experimentation.

The widely used XBee3 module evaluated in this work has an advertised effective operating range of 1200 m [18], but, as our evaluation shows, variables such as altitude of UAS, antenna type, antenna orientation (of transmitter and receiver), evaluation, and obstruction can dramatically limit the maximum horizontal displacement with a usable PRR. Moreover there is not a one size fits all configuration.

For an outdoor grassland setting, results show that if the

UAS flight plan is expected to come close to the transmitters ($< 150m$), then an altitude of 150-250 ft with internal antennae consisting of an elevated vertical transmitter and a horizontal receiver produce the best PRR. For effective data collection at greater displacements ($> 150m$), external antennae consisting of a vertical transmitter and a vertical receiver are optimal regardless of flight altitude.

In our experiment packets were broadcast by the transmitters at a rate of 500 ms, which is highly energy intensive for deployments that might need to operate on battery power for weeks or months. Unfortunately, experimentation on lowering transmission rate proved challenging due to the power

requirements of the UAS. As each UAS battery provides just over 20 minutes of useful flight, experimentation on slow transmission rates makes collection of a meaningful amount of data challenging. Initial results showed that the UAS would have to slow flight speed substantially for slower transmission rates. To address this issue there is active research on using low power radios for "waking" 802.15.4 radios for transmission [20].

While our dataset will likely not generalize to all terrain and geographies (e.g. an urban sensor deployment), we believe our method of modeling and insights into three dimensional performance of 2.4GHz 802.15.4 under a variety of antenna configurations is highly transferable to future work in 802.15.4 analysis and to real-world sensor network planning.

ACKNOWLEDGMENTS

REFERENCES

[1] I. Howitt and J. A. Gutierrez, "IEEE 802.15.4 low rate - wireless personal area network coexistence issues," in *IEEE Wireless Communications and Networking (WCNC)*, vol. 3, March 2003.

[2] B. P. Fitzpatrick, "Unmanned Aerial Systems for Surveying and Mapping: Cost Comparison of UAS Versus Traditional Methods of Data Acquisition," Ph.D. dissertation, University of Southern California, 2015.

[3] J. Torres-Sánchez, F. López-Granados, N. Serrano, O. Arquero, and J. M. Peña, "High-throughput 3-D monitoring of agricultural-tree plantations with unmanned aerial vehicle (UAV) technology," *PLOS ONE*, vol. 10, no. 6, June 2015.

[4] M. Nekrasov, R. Allen, and E. Belding, "Performance analysis of aerial data collection from outdoor IoT sensor networks using 2.4 GHz 802.15.4," in *Proceedings of the 5th Workshop on Micro Aerial Vehicle Networks, Systems, and Applications*. ACM, 2019, pp. 33–38.

[5] C. Lima, E. Silva, and P. Velloso, "Performance evaluation of 802.11 IoT devices for data collection in the forest with drones," in *GLOBECOM*. IEEE, 2018.

[6] M. Asadpour, D. Giustiniano, and K. A. Hummel, "From ground to aerial communication: Dissecting WLAN 802.11n for the drones," in *WiNTECH*. ACM, 2013, pp. 25–32.

[7] E. Yanmaz, R. Kuschnig, and C. Bettstetter, "Channel measurements over 802.11a-based UAV-to-ground links," in *GLOBECOM*. IEEE, 2011.

[8] C.-M. Cheng, P.-H. Hsiao, H. Kung, and D. Vlah, "Performance measurement of 802.11a wireless links from UAV to ground nodes with various antenna orientations," in *ICCCN*. IEEE, 2006, pp. 303–308.

[9] S. Hara, D. Zhao, K. Yanagihara, J. Taketsugu, K. Fukui, S. Fukunaga, and K.-i. Kitayama, "Propagation characteristics of IEEE 802.15.4 radio signal and their application for location estimation," in *Vehicular Technology Conference*, vol. 1. IEEE, 2005, pp. 97–101.

[10] E. Miluzzo, X. Zheng, K. Fodor, and A. T. Campbell, "Radio characterization of 802.15.4 and its impact on the design of mobile sensor networks," in *EWSN*. Springer, 2008, pp. 171–188.

[11] M. Khanafer, M. Kandil, R. Al-Baghdadi, A. Al-Ajmi, and H. T. Mouftah, "Enhancements to IEEE 802.15.4 MAC protocol to support vehicle-to-roadside communications in VANETs," in *IEEE International Conference on Communications (ICC)*, May 2019.

[12] M. Petrova, J. Riihijarvi, P. Mahonen, and S. Labella, "Performance study of IEEE 802.15.4 using measurements and simulations," in *WCNC*, vol. 1. IEEE, 2006, pp. 487–492.

[13] D. Lymberopoulos, Q. Lindsey, and A. Savvides, "An empirical characterization of radio signal strength variability in 3-D IEEE 802.15.4 networks using monopole antennas," in *EWSN*. Springer, 2006, pp. 326–341.

[14] Y. Qin, D. Boyle, and E. Yeatman, "Efficient and reliable aerial communication with wireless sensors," *IEEE Internet of Things Journal*, vol. 6, no. 5, Oct 2019.

[15] R. Kirichek and V. Kulik, "Long-range data transmission on flying ubiquitous sensor networks (FUSN) by using LPWAN protocols," in *Distributed Computer and Communication Networks*. Springer International Publishing, 2016.

[16] J. R. Martinez-de Dios, K. Lferd, A. de San Bernabé, G. Núñez, A. Torres-González, and A. Ollero, "Cooperation between UAS and wireless sensor networks for efficient data collection in large environments," *Journal of Intelligent & Robotic Systems*, vol. 70, 2013.

[17] M. Nekrasov, R. Allen, I. Artamonova, and E. Belding, "Optimizing 802.15.4 outdoor IoT sensor networks for aerial data collection," *Sensors*, vol. 19, no. 16, 2019.

[18] Digi, "XBee3 Zigbee 3.0 datasheet," https://www.digi.com/pdf/ds_xbee-3zigbee3.pdf, 2019.

[19] Chang Hong Technology Co., "2.4G Dipole 2dBi Antenna," https://www.sparkfun.com/datasheets/Wireless/Antenna/DA-24-04.pdf, Feb. 2007.

[20] S. Basagni, F. Ceccarelli, C. Petrioli, N. Raman, and A. V. Sheshashayee, "Wake-up radio ranges: A performance study," in *2019 IEEE Wireless Communications and Networking Conference (WCNC)*. IEEE, 2019.